Experimental Neurology 314 (2019) 82–90

Contents lists available at ScienceDirect

Experimental Neurology

journal homepage: www.elsevier.com/locate/yexnr

Research paper

# Characterization of leptomeningeal inflammation in rodent experimental autoimmune encephalomyelitis (EAE) model of multiple sclerosis

Suyog Pol[a], Ferdinand Schweser[a,b], Nicola Bertolino[a], Marilena Preda[a], Michele Sveinsson[a], Michelle Sudyn[a], Natan Babek[a], Robert Zivadinov[a,b,*]

[a] Buffalo Neuroimaging Analysis Center, Department of Neurology, Jacobs School of Medicine and Biomedical Sciences, University at Buffalo, State University of New York, Buffalo, NY, USA
[b] Center for Biomedical Imaging at Clinical Translational Science Institute, University at Buffalo, State University of New York, Buffalo, NY, USA

ARTICLE INFO

*Keywords:*
EAE
MRI
Leptomeningeal enhancement
Multiple sclerosis
Inflammation

ABSTRACT

*Background:* Leptomeningeal inflammation, as evidenced by leptomeningeal contrast enhancement (LMCE), is associated to cortical pathology in multiple sclerosis. The temporal pattern of LMCE in experimental autoimmune encephalomyelitis (EAE) myelin oligodendrocyte glycoprotein (MOG) is unknown.
*Objective:* To investigate LMCE using serial MRI in the EAE model of MS, and its association with clinical disease progression. To characterize the relationship between LMCE and underlying histological correlates.
*Design:* Thirteen C57BL/6J mice, MOG-immunized (35–55 amino acid) and 8 saline injected animals were assessed at pre-induction and at 3, 6, 10, 20, 27, 32, 45 and 63 days post induction (dPI). LMCE scan was obtained using FLAIR-RARE sequence after post-contrast gadolinium administration on 9.4 T scanner. Brain cryo-sections were assessed for measuring cellular density of Iba1 positive macrophage/microglia at 10 dPI and 32 dPI, and for the presence of T, B and macrophage cells in the meningeal layer at 10 dPI and 63 dPI.
*Results:* All EAE-MOG animals showed presence of LMCE and none of the control mice. The peak signal intensity of LMCE was evidenced at 10dPI in the meninges and decreased through 10–63 dPI. The peak of LMCE was associated with a weight loss starting at 1 week PI and with clinical symptoms starting at 2 weeks PI. Histological analysis of the brain tissue showed a higher density of Iba1 positive microglial cells in the EAE-MOG animals, corresponding to the areas of LMCE. Meninges of EAE mice showed higher density of Iba1 stained macrophage cells relative to saline animals. EAE animals also showed the presence of T and B cells in the meninges which were absent in the saline animals.
*Conclusions:* LMCE peak intensity in the meninges corresponds to the acute inflammatory phase of EAE-MOG disease progression, and is associated with clinical symptoms and higher inflammatory cell density.

## 1. Introduction

In clinical setting, leptomeningeal contrast enhancement (LMCE) is detectable on MRI, and was proposed to represent a compartmentalized inflammation in multiple sclerosis (MS) patients (Absinta et al., 2015). LMCE has been shown to be the site of persistent follicular structures harboring inflammatory cells within the subarachnoid space, responsible for sustaining neurodegeneration in brain (Absinta et al., 2015; Bertolino et al., 2017; Harrison et al., 2017; Makshakov et al., 2017; Zivadinov et al., 2018). MS patients with presence of LMCE are more likely to develop cortical grey matter atrophy over long-term (Bertolino et al., 2017; Makshakov et al., 2017). However, LMCE-detected follicular structure formation and its exact relationship with the disease progression are not well understood (Absinta et al., 2015), and the identification of a matching phenomenon in the preclinical setting is an open challenge due to the difference in the human and rodent brain disease models (Dietz et al., 2016). Thus taking LMCEs clinical relevance and research implications into consideration, we sought to establish this imaging methodology in a pre-clinical model of demyelination.

Targeted autoimmune process mediated disruption of central nervous system (CNS) myelin is the primary driver of MS disease etiology (McFarland and Martin, 2007). Cellular mechanisms and cellular infiltration gateways into immune isolated brain parenchyma remain a

* Corresponding author at: Buffalo Neuroimaging Analysis Center, Center for Biomedical Imaging at Clinical Translational Science Institute, University at Buffalo, State University of New York, 100 High Street, Buffalo, NY 14203, USA.
*E-mail address:* rzivadinov@bnac.net (R. Zivadinov).

https://doi.org/10.1016/j.expneurol.2019.01.013
Received 17 April 2018; Received in revised form 14 January 2019; Accepted 21 January 2019
Available online 23 January 2019
0014-4886/ 

topic of intense research in MS. Leukocytes have been hypothesized to infiltrate the CNS through interfaces separating vascular and lymphatic systems at one side, and CNS subarachnoid space and circulating cerebrospinal-fluid on the other (Louveau et al., 2015; Ransohoff et al., 2003). Several mechanisms have been suggested to model this process based on neuroimaging and histological data (Kivisakk et al., 2009; Petry et al., 2010). Additionally, it has been hypothesized that alternate mechanisms may be active in parallel or in tandem (Ransohoff et al., 2003; Ladewig et al., 2009). However, due to the unpredictable disease course of MS, a characterization of the exact chronology of the above events non-invasively in a clinical setting remains technically challenging (Petry et al., 2010).

To this end, imaging of iron-oxide based contrast agents (CA) carrying inflammatory cells, has been applied to trace their CNS infiltration route into experimental autoimmune encephalomyelitis (EAE) brains (Ladewig et al., 2009; Fournier et al., 2017; Mardiguian et al., 2013; Stoll and Bendszus, 2009; Weise and Stoll, 2012). In parallel, gadolinium-based CAs are being developed to identify sites of blood-brain-barrier (BBB) breakdown and lesion formation with higher sensitivity (Mardiguian et al., 2013). Gadolinium-based and iron oxide-based CAs were also used in combination to understand if BBB breakdown, leukocyte infiltration and lesion formation are spatiotemporally correlated (Ladewig et al., 2009; Stoll and Bendszus, 2009). The results from these studies have largely been inconsistent with each other (Ladewig et al., 2009; Stoll and Bendszus, 2009; Weise and Stoll, 2012). On the other hand, these studies did not characterize the initial accumulation of gadolinium CA within the meninges, which mirrors the initial steps in the inflammation and breakdown of BBB.

To this end, a neuroimaging based approach was first developed to longitudinally trace EAE disease progression within the same animal in vivo using a gadolinium-based CA scanning protocol on an ultra-high field 9.4 T small animal scanner. The aims of the study were to investigate patterns of LMCE using serial MRI in the EAE model of MS, and its association with clinical symptoms and disease progression. We also characterized the relationship between LMCE and the presence of immune cells at the brain meninges.

## 2. Methods

### 2.1. EAE induction procedure and clinical monitoring

All protocols were approved by Institutional animal care and use (IACUC). Animals were housed in a temperature-controlled room maintained on a 12 h light/dark cycle. Food and water were available ad libitum. The animal facility was fully accredited by the Association for Assessment and Accreditation of Laboratory Animal Care (AAALAC) International.

We immunized 7–8 week old female C57BL/6J mice with myelin oligodendrocyte glycoprotein ($MOG_{35–55}$) peptide fragment with a subcutaneous axillary injection at the flanks twice. Four ($n = 4$) and further additional 9 animals, for a total of 13 animals, were injected with 150 μg and 250 μg of MOG, respectively. Controls were injected with saline ($n = 8$). The first injection date was considered day zero. For $MOG_{35–55}$ injections, the peptide was emulsified in 50 μl phosphate buffer solution (PBS) and 50 μl of incomplete Freud's adjuvant with 1 mg/μl inactive M. tuberculosis. The animals were intra-peritoneally injected with 500 ng of pertussis toxin after MOG injection and once more 2 days later (Jones et al., 2008). The animals were weighted and monitored daily after MOG immunization. Clinical disability scores were assigned on a 5 point scale where, 0 denotes no deficit, 0.5 abnormal gait or tail tone loss, 1.0: complete tail paralysis or tail tone loss with abnormal gait, 1.5 complete tail paralysis and mild hind limb weakness, 2.0 tail paralysis with moderate hind limb weakness, 2.5 no weight-bearing on hind limbs some movement, 3.0 complete hind limb paralysis, 3.5 weakness in forelimbs, 4.0 complete quadriplegia, and 4.5 moribund. To validate disease induction, clinical disability score and body weight were recorded daily post-induction (dPI).

### 2.2. MRI image acquisition

3–4% isofluorane was used for anesthesia induction and 1–2% was used for maintenance. Animals were scanned with a 20 cm diameter horizontal-bore 9.4T (Biospec 94/20 USR, Bruker Biospin) operated with ParaVision (version 5.1; Bruker Biospin) and equipped with a gradient coil supporting 440 mT/m gradient strength and 3440 T/m/s maximum linear slew rate. We employed a cross-coil configuration with a 4-channel receiver surface coil and a quadrature transmitter volume coil. An axial 2D fluid attenuated inversion recovery (FLAIR) pulse sequence was generated by adding an inversion recovery module to a Rapid Acquisition with Refocused Echoes (RARE) sequence (Bertolino et al., 2017) (FLAIR-RARE: TR/TE = 3500/5.44 ms; RARE-factor = 2; averages = 3; 22 slices of 600 μm; matrix = 170 × 180; 2× zero-filled in-plane resolution = 52.5 × 52.5$\mu m^2$; TA = 15m45s). We set the inversion time (TI) to 1162 ms to null signal from cerebrospinal fluid (CSF) ($T1_{CSF}$ = 2450 $ms^{10}$ at 9.4 T). We repeated the FLAIR-RARE sequence three times consecutively after the post tail-vein injection of 0.2 μmol/g gadobutrol. The second FLAIR-RARE scan (20 mins post-contrast injection) was found to have highest contrast signal and was used for further analysis. To observe entire LMCE evolution during EAE disease course, the animals were scanned approximately twice every week i.e. baseline, 3, 6, 10, 20, 27, 32, 45 and 63 dPI. The scan timepoints and number of animals per scan timepoint are as specified in Table 1.

### 2.3. MRI image analysis

All MRI images were transformed using N4 bias field correction algorithm and normalized using histogram matching algorithm to a reference image using ANTs tools. MRI images were visualized in 3D Slicer software (version 4.3). Regions of interests (ROI) label files were generated using label editor module. For measuring meningeal signal intensity, a 2 voxel wide label was generated at the meninges

**Table 1**
Disposition of animals used for MRI scanning and histological analysis for each of the study timepoints.

| | | Study timepoints (dPI) | | | | | | | | |
|---|---|---|---|---|---|---|---|---|---|---|
| | | Baseline | 3 | 6 | 10 | 20 | 27 | 32 | 45 | 63 |
| MRI | EAE ($n = 13$) (150 μg\|250 μg) | 4\|9 | 3\|0 | 3\|0 | 4\|8 | 3\|0 | 6\|0 | 3\|0 | 0\|4 | 0\|3 |
| | Saline (n-8) | 6 | 2 | 2 | 4 | 2 | 2 | 4 | 5 | 5 |
| Histology | EAE ($n = 11$) (150 μg\|250 μg) | – | – | – | 4\|0 | – | – | 4\|0 | – | 0\|3 |
| | Saline ($n = 4$) | – | – | – | – | – | – | 4 | – | – |

**Legend:** EAE-experimental autoimmune encephalomyelitis; dPI-days post induction.
For EAE mice details, mice injected with different MOG doses are separately indicated.

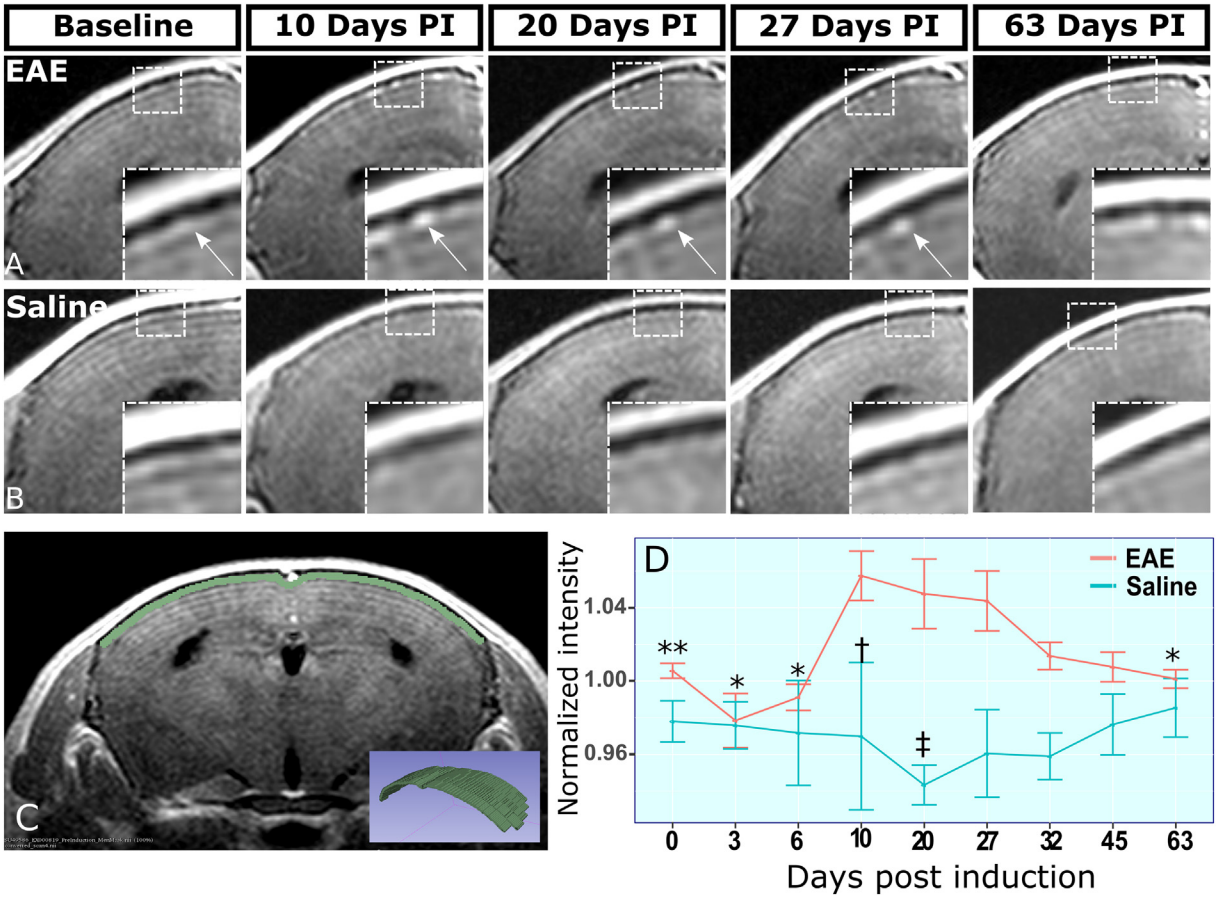


**Fig. 1.** Experimental autoimmune encephalomyelitis myelin oligodendrocyte glycoprotein (EAE-MOG) animals exhibit gadolinium-based contrast agent signal intensity at the meninges.
(A) shows representative stage matched slices from EAE-MOG animal brain scans with peak gadolinium-based CA signal during early disease state. The arrow points at nodule like structure which commonly appeared at early phase of the disease and remained stable through the disease course. (B) shows control animal brain scans at corresponding timepoints. Inset is showing enlarged view of the meninges. (C) shows the placement of 4 voxel wide region of interest at the dorsal meninges of brain on 5 consecutive slices spanning the mid forebrain. The inset is a 3D rendering of the region of interest. (D) shows graphs the voxel-wise mean signal intensity within the region of interest for each animal within the study. * $p < .05$ and ** $p < .01$, *Students t-test for comparison with 10 dPI EAE signal.* † $p < .05$ and, ‡ $p < .01$, *Students t-test for EAE* vs *saline comparisons at matching timepoints. Error bars: Standard error of the mean.*

underneath the parietal-cranial bone in 5 consecutive slices (Fig. 1C). For measuring the background signal, a 5 voxel wide label was placed within the brain adjacent to the above meninges label. For quantification of sagittal sinus, a 4 voxel diameter label was placed at the center of the sagittal sinus in three consecutive slices starting from slice with visible fimbria. Finally, for a quantification of signal in the longitudinal sulcus, a 2 voxel wide label was placed in the hyperintensity visible at the longitudinal sulcus in slice with visible fimbria. The label-specific voxel signal intensities were quantified using the label statistics tool. For measuring the background signal for sagittal sinus and longitudinal sulcus, a 2 voxel wide label was placed on brain tissue adjacent to the respective labels. All label-wise mean signal values were normalized by division with mean signal value measured in respective background tissue labels.

### 2.4. Brain tissue isolation and immunostaining

Within 48 h after last MRI, the animals received a fatal dose of pentobarbital and were intracardially perfused the first 15 min with 0.9% saline solution and then 15 min with 4% para-formaldehyde solution. The number of animals sacrificed at baseline, 10dPI, 32 dPI and 63dPI in each group are specified in Table 1. We extracted the brains and placed them in PBS, 6% sucrose PBS solution, and 16% PBS solution sequentially for one night each. Following this, we flash froze the brains using a dry ice-ethanol bath. We serially cryosectioned (16 µm thick) the cryopreserved brains, collected sections on microscope slides, and stored them at −80 °C. The above sections were brought to room temperature and washed three times with PBS solution (Abiraman et al., 2015). We permeabilized the sections for 15 min (1% TritonX-100 (Sigma) and 0.25% Tween-20 (Sigma) in PBS), blocked them for 1 h (1% TritonX-100, 25% Goat Serum (ThermoFisher, USA) in PBS), and incubated them with rabbit anti Iba1 antibody (Wako Pure Chemical Industry Ltd., Japan) at 1:400 dilution, CD19 (Biolegend) antibody at 1:100 dilution, CD45 (Biolegend) antibody at 1:100 dilution overnight. For labeling with secondary antibody, we incubated the sections with goat anti-rabbit Alexa 594 or an Alexa 488 secondary antibody at 1:500 dilution for Iba1 staining, and goat anti rat Alexa 488 for CD19&CD45 staining (ThermoFisher, USA). The slides were sealed with ProlongGold (Thermofisher, USA) mounting reagent and imaging were taken at 200× magnification each, on Zeiss fluorescent microscope operated by Zen Blue (Zeiss, Germany). Histology images were quantified for Iba1 positive stained cells with the ImageJ software (version 4.0) (Ito et al., 1998).

### 2.5. Statistical analysis

For statistical analysis and graphical presentation we used the R programming language (version 3.3). Label-wise mean intensity values

between 10dPI were compared to other time points using two tailed Student's *t*-test. Student's t-test was used for comparing EAE vs. control label-wise mean signal intensity. Spearman's correlation between signal intensity and disease stages was conducted to measure significance and rho (ρ) value. Clinical scores between different timepoints within the EAE group were compared using Wilcoxon ranked sum test. All histological cell density measures comparisons were performed using with Student's t-test. A nominal *p*-value of $< 0.05$ was considered statistically significant, and $p < .1$ was considered a trend, using two-tailed tests.

## 3. Results

### 3.1. Leptomeningeal contrast enhancement detection

LMCE signal was increased in the meninges of EAE-MOG brains, compared to control animals (Fig. 1A–B). Close observation of the images also revealed nodule like hyper-intensities in the meninges of the EAE-MOG animals, which were stable through the disease course (Fig. 1A, **insets**).

The measured label-wise normalized mean signal, i.e. LMCE signal intensity, in the meningeal region of the mice changed with time, with peak signal at 10 dPI (1.005 ± 0.005 SEM at baseline vs. 1.059 ± 0.016 SEM 10dPI in EAE, $p = .002$, Table 2). By 45dPI the normalized signal in the meninges trended lower (1.008 ± 0.008 SEM at 45dPI vs. 1.059 ± 0.016 SEM 10dPI in EAE, $p = .09$, Table 2). By day 63 PI, the signal intensity trended lower relative to day 10 dPI ($p = .097$), and was comparable to control animals (1.001 ± 0.005 SEM in EAE vs. 0.985 ± 0.016 SEM in saline at 63dPI, $p = .496$, Table 2).The normalized mean LMCE signal intensity in the meninges in the EAE-MOG mice was significantly higher in comparison to control animals at 10 dPI (Fig. 1D) (1.059 ± 0.016 SEM 10dPI in EAE vs. 0.970 ± 0.040 SEM in saline, $p = .024$).

### 3.2. Leptomeningeal contrast enhancement correlates with disease activity

The animals exhibited initial symptoms such as drooping tail, starting at approximately 10–13 dPI. We detected corresponding increment in the scores of clinical disability at 14–21 dPI (0.07 ± 0.18 SEM at 0dPI vs 1.42 ± 1.01 SEM at 20 dPI, $p < .05$) (Fig. 2A) and after this time period the clinical disabilities remained stable. This divided the disease course into distinct early (1 to 10 dPI), acute (10 to 20 dPI) and chronic phase (20 to 63 dPI) (Fig. 2A). Similarly, we noticed a trend of decrease in body weight starting at 7 dPI in the EAE-MOG animals (Fig. 2B). Saline animals did not exhibit any clinical disability and abnormal body weight changes.

We found a significant positive correlation between the LMCE signal intensity and the time of early disease phase ($\rho = 0.485$, $p = 0009$, Spearmans Correlation), followed by a trend of negative correlation with the chronic disease phase ($\rho = -0.488$, $p = .055$, Spearman's Correlation) (Fig. 2C–E, Table 3).

### 3.3. EAE brain subpial cortical and meningeal tissue histological analysis indicates higher immune activity

We found that there was a significantly higher density of the Iba1 positive cells in the subpial cortical layer in EAE-MOG animal brains isolated at 32 dPI, compared with saline injected animal brains (35.70 ± 3.24 SEM EAE 10 dPI vs. 26.5 ± 5.17 SEM Saline, $p < .05$, Fig. 2F & H, Table 4). Interestingly, density of Iba1 positive cells in the subpial cortical layer was even higher in the animal brains isolated at 10 dPI, compared with EAE-MOG brains isolated at 32 dPI (91.36 ± 20.49SEM 10dPIvs. 35.71 ± 3.24SEM 32dPI, $p < .05$, Fig. 2F & G, Table 4). At 63 days PI, the density of the Iba1 positive cells was still higher compared to saline animals, but not significantly different (33.3 ± 4.48SEM in EAE vs. 26.5 ± 5.17 SEM in saline, Fig. 2F & I, Table 4). Thus, the measured density of Iba1 labeled cells was in agreement with the longitudinal changes of the LMCE signal.

Additionally, MRI signal positive EAE brain meningeal layer was immunostained for detecting CD45, CD19 and Iba1 expressing cells for qualitative characterization. (Fig. 3). We found that EAE mouse meninges presented clusters of Iba1 positive macrophage cells compared to sporadic distribution of Iba1 expressing cells in saline injected animal meninges (Fig. 3A–C). We observed that EAE mouse brain meninges presented a sporadic distribution of cells expressing CD45 (Fig. 3D–F) and CD19 (Fig. 3G–I), which were not detected in saline injected control animal meninges.

### 3.4. Leptomeningeal contrast enhancement localizes with inflamed brain vasculature and other sites of inflammation on brain surface

In addition to the meninges, we found that gadolinium-based CA signal intensity was visibly different in other EAE-MOG brain regions as well, compared to control animals and PI baseline scans. Therefore, we sought to characterize these signal intensity changes further.

The superior sagittal sinus (Fig. 4J), which is a vein responsible for draining away blood supplied to the anterior hemispheres of the cerebrum, (Dorr et al., 2007) presented temporally increasing amount of gadolinium-based CA generated signal (Fig. 4B, red arrow). This was observable in all the image slices encompassing the superior sagittal sinuses. We found that the signal intensity was significantly higher in the EAE-MOG animal brains and the peak signal intensity coincided with inflammatory phase of the disease (1.449 ± 0.060 SEM at baseline vs. 1.792 ± 0.099 SEM 10dPI in EAE, $p = .006$, Fig. 4I, Table 2). At 63 dPI, the signal intensity in EAE was comparable to the signal intensity in saline animals (1.554 ± 0.136 SEM in EAE vs. 1.481 ± 0.060 SEM in in saline animals at 63dPI, $p = .588$, Fig. 4I, Table 1).

Longitudinal sulcus (Fig. 4L) separates two cerebral hemispheres of the brain. In addition to the higher gadolinium-based CA signal in veins, we found that the longitudinal sulcus also had a higher signal intensity (Fig. 4A–D, green arrow). The quantification of the mean voxel-wise signal intensity showed that EAE-MOG animals had higher signal intensity retention in this area compared to baseline (1.056 ± 0.017 SEM at baseline vs. 1.306 ± 0.041 SEM 10dPI in EAE, $p < .001$, Fig. 4A, B & K, Table 2). Signal intensity measure in longitudinal sulcus had highest correlation with early disease phase in comparison to the other measured regions ($\rho = 0.736$, $p = 8.04 \times 10^{-6}$, Spearmans Correlation). At 63 dPI, the signal intensity in EAE was comparable to the signal intensity in saline animals (1.086 ± 0.002 SEM in EAE vs. 1.067 ± 0.019 SEM in in saline animals at 63dPI, $p = .477$, Fig. 4A, D & K, Table 2,).

Brain tissue sections immune-stained for Iba1 were also analyzed to investigate, if early EAE longitudinal sulcus was associated with greater density of immune cells (Fig. 3) [19]. We detected a significantly higher density of the Iba1 positive cells in the meninges in EAE-MOG animal brains isolated at 32 dPI, compared with saline ones. Interestingly, we found that the density of Iba1 positive cells in the meninges was even higher in the animal brains isolated at 10 dPI, compared with EAE-MOG brains isolated at 32 dPI (50.375 ± 9.42 SEM 10dPI vs. 30.909 ± 2.32 SEM 32dPI, $p < .05$, Fig. 4F & G, Table 4). The saline animals had significantly lower Iba1 stained cells at long sulcus (16.43 ± 2.42 SEM, Table 4). At 63 days PI, the density of the Iba1 positive cells was still significantly higher than in the saline animals (33.3 ± 4.48SEM in EAE vs. 26.5 ± 5.17 SEM in saline, $p < .05$, Fig. 4H & E, Table 4). Additionally, the density of Iba1 stained cells in EAE brain steadily decreased with distance further away from the long sulcus towards inner brain tissue.

## 4. Discussion

We investigated a longitudinal serial tracking of gadolinium-based

**Table 2**
Label-wise mean signal intensity of gadolinium-based contrast agent in various brain structures in EAE and saline mice at different time points of the study.

| Regions | Condition | Timepoint (dPI) | Mean | N | SEM | | |
|---|---|---|---|---|---|---|---|
| Meninges | | | | | | **pValue vs Baseline** | **pValue vs 10dpi** |
| | **EAE** | 0 | 1.005 | 13 | 0.005 | – | **0.002** |
| | | 3 | 0.978 | 3 | 0.015 | **0.041** | **0.03** |
| | | 6 | 0.991 | 3 | 0.007 | 0.208 | 0.057 |
| | | 10 | 1.059 | 12 | 0.016 | **0.002** | **–** |
| | | 20 | 1.048 | 3 | 0.019 | **0.005** | 0.733 |
| | | 27 | 1.044 | 6 | 0.016 | **0.007** | 0.547 |
| | | 32 | 1.014 | 3 | 0.007 | 0.412 | 0.186 |
| | | 45 | 1.008 | 4 | 0.008 | 0.774 | 0.09 |
| | | 63 | 1.001 | 3 | 0.005 | 0.719 | 0.097 |
| | | | | | | **pValue vs EAE** | |
| | **Saline** | 0 | 0.978 | 6 | 0.011 | – | 0.272 |
| | | 3 | 0.976 | 2 | | – | – |
| | | 6 | 0.972 | 2 | | – | – |
| | | 10 | 0.970 | 4 | 0.040 | **0.024** | |
| | | 20 | 0.943 | 2 | | – | – |
| | | 27 | 0.961 | 2 | | – | – |
| | | 32 | 0.959 | 4 | 0.013 | **0.02** | 0.805 |
| | | 45 | 0.976 | 5 | 0.017 | 0.163 | 0.876 |
| | | 63 | 0.985 | 5 | 0.016 | 0.496 | 0.706 |
| Sagittal sinus | | | | | | **pValue vs Baseline** | |
| | **EAE** | 0 | 1.449 | 13 | 0.060 | – | **0.006** |
| | | 3 | 1.485 | 3 | 0.073 | 0.79 | 0.159 |
| | | 6 | 1.524 | 3 | 0.023 | 0.573 | 0.21 |
| | | 10 | 1.792 | 12 | 0.099 | **0.006** | **–** |
| | | 20 | 1.508 | 3 | 0.124 | 0.681 | 0.199 |
| | | 27 | 1.442 | 6 | 0.126 | 0.954 | 0.051 |
| | | 32 | 1.512 | 3 | 0.030 | 0.633 | 0.192 |
| | | 45 | 1.537 | 4 | 0.068 | 0.463 | 0.175 |
| | | 63 | 1.554 | 3 | 0.136 | 0.47 | 0.28 |
| | | | | | | **pValue vs EAE** | |
| | **Saline** | 0 | 1.483 | 6 | 0.039 | 0.726 | 0.435 |
| | | 3 | 1.546 | 2 | 0.110 | – | – |
| | | 6 | 1.432 | 2 | 0.040 | – | – |
| | | 10 | 1.398 | 4 | 0.115 | 0.052 | – |
| | | 20 | 1.379 | 2 | 0.164 | – | – |
| | | 27 | 1.298 | 2 | 0.027 | – | – |
| | | 32 | 1.342 | 4 | 0.097 | 0.207 | 0.719 |
| | | 45 | 1.466 | 5 | 0.088 | 0.563 | 0.646 |
| | | 63 | 1.481 | 5 | 0.060 | 0.588 | 0.519 |
| Longitudinal sulcus | | | | | | **pValue vs Baseline** | |
| | **EAE** | 0 | 1.056 | 13 | 0.017 | – | > **0.001** |
| | | 3 | 1.101 | 3 | 0.067 | 0.343 | **0.039** |
| | | 6 | 1.149 | 3 | 0.046 | **0.037** | 0.095 |
| | | 10 | 1.306 | 12 | 0.041 | > **0.001** | **–** |
| | | 20 | 1.223 | 3 | 0.012 | > **0.001** | 0.346 |
| | | 27 | 1.247 | 6 | 0.052 | > **0.001** | 0.403 |
| | | 32 | 1.170 | 3 | 0.045 | **0.013** | 0.143 |
| | | 45 | 1.206 | 4 | 0.038 | > **0.001** | 0.21 |
| | | 63 | 1.086 | 3 | 0.002 | 0.414 | **0.022** |
| | | | | | | **pValue vs EAE** | |
| | **Saline** | 0 | 1.036 | 6 | 0.017 | 0.451 | 0.183 |
| | | 3 | 0.980 | 2 | 0.039 | – | – |
| | | 6 | 1.026 | 2 | 0.015 | – | – |
| | | 10 | 1.107 | 4 | 0.056 | **0.024** | – |
| | | 20 | 1.051 | 2 | 0.003 | **–** | 0.539 |
| | | 27 | 1.073 | 2 | 0.006 | – | 0.708 |
| | | 32 | 1.057 | 4 | 0.028 | 0.073 | 0.455 |
| | | 45 | 1.034 | 5 | 0.023 | **0.005** | 0.229 |
| | | 63 | 1.067 | 5 | 0.019 | 0.477 | 0.479 |

EAE-experimental autoimmune encephalomyelitis; N-number animals, SEM-standard error mean; dPI-days post induction. Mean and SEM for voxel-wise mean signal intensity was measured in the three regions of interest i.e. meninges, longitudinal sulcus and sagittal sinus. “vs baseline” column represents baseline vs follow-up timepoint comparison (Student's t-test) within EAE animal measurements. “vs EAE” columns reoresent EAE and Saline valid comparisons (Student's *t*-test) for matching timepoints. “vs 10dPI” reports valid comparisons (Student's t-test) with 10 dPI within each group. The $p$ values $< .05$ are shown in bold.
Because not all subjects obtained imaging at all time points, p values were not possible to be obtained for some time points. In addition, p values were not obtained when comparisons included the same time point for same subjects.

CA generated signal in the EAE-MOG brain's inflammatory surface using ultra-high field MRI. The gadolinium-based CA signal was observed at various sites of inflammation i.e. at the meninges, sagittal sinus and longitudinal sulcus with each region exhibiting signal intensity temporal changes. Furthermore, the MRI detected signals were consistent with early stages of the disease and underlying inflammatory histology. The MRI signal enhancement was less pronounced through the later (32 dPI to 63dPI) study timepoints.

Previous mouse brain neuroimaging studies investigating BBB integrity in EAE brains post gadolinium-based CA injection, showed

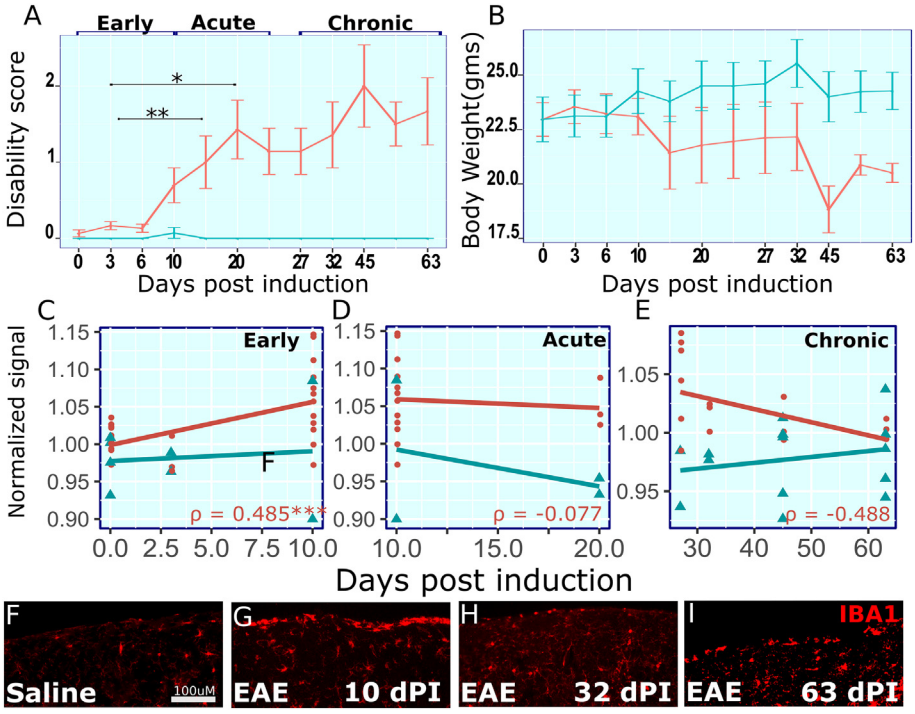


**Fig. 2.** Experimental autoimmune encephalomyelitis myelin oligodendrocyte glycoprotein (EAE-MOG) animal's clinical disability correlates with MRI gadolinium-based contrast agent signal intensity at meninges. (A) The animals were daily monitored for assessment of their disability on the IDSS scale. The early increase in the measured disability peaked at day 10 for EAE induced animals. (B) The body weight showed a non-significant declining trend in the weights starting at day 6 but recovered to normal control levels. To understand the relationship between the different stages of the disease we obtained correlations between the three different stages of the disease. (C) represents early phase, (D) acute phase, and (E) chronic phase of the disease. The Spearman correlation ρ value is reported in the graph for the EAE animals. (F) brain sections from the regions shown in F–I were stained for marker of microglial cells and inflammatory immune cells. Note the higher density of microglial cells in the subpial region at the 10 day timepoint. * $p < .05$ and ** $p < .01$, 's t-test for EAE. Error bars: Standard error of the mean. Student t-test was used for body weight and Wilcoxs rank sum test was used for clinical score in EAE vs saline comparisons. Error bars: Standard error of the mean. The early, acute and the chronic phases of the disease have been indicated in the timeline. Scale is 100 μm.

**Table 3**
Correlation of MRI signal with disease state.

| Regions | Condition | Disease state | Correlation | N | P value |
|---|---|---|---|---|---|
| Meninges | EAE | Early | 0.485 | 3 | 0.009 |
| | | Acute | −0.077 | 3 | 0.785 |
| | | Chronic | −0.489 | 3 | 0.055 |
| | Saline | Early | −0.077 | 3 | 0.856 |
| | | Acute | 0.000 | 3 | 1.000 |
| | | Chronic | 0.286 | 3 | 0.322 |
| Sagittal sinus | EAE | Early | 0.502 | 3 | 0.006 |
| | | Acute | −0.386 | 3 | 0.156 |
| | | Chronic | 0.326 | 3 | 0.218 |
| | Saline | Early | 0.000 | 3 | 1.000 |
| | | Acute | −0.447 | 3 | 0.553 |
| | | Chronic | 0.381 | 3 | 0.179 |
| Longitudinal sulcus | EAE | Early | 0.736 | 3 | 8.04E-06 |
| | | Acute | −0.347 | 3 | 0.205 |
| | | Chronic | −0.484 | 3 | 0.055 |
| | Saline | Early | 0.000 | 3 | 1.000 |
| | | Acute | 0.000 | 3 | 1.000 |
| | | Chronic | −0.125 | 3 | 0.671 |

EAE-experimental autoimmune encephalomyelitis; N-number animals. For measuring correlation with disease phase, voxel-wise mean MRI signal data point were subset into early (baseline to 10dPI), acute (10 dPI to 20 dPI) and chronic (20 dPI to 32 dPI) disease phase. Correlation was measured using Spearmans correlation (ρ).
Because not all subjects obtained imaging at all time points, p values were not possible to be obtained for some time points. In addition, p values were not obtained when comparisons included the same time point for same subjects.

**Table 4**
Mean density of Iba1 expressing cells.

| Regions | Condition | Timepoint (dPI) | Density | N | SEM |
|---|---|---|---|---|---|
| Subpial Cortex | EAE | 10 | 91.4 | 3 | 10.37 |
| | | 32 | 35.7 | 4 | 3.25 |
| | | 63 | 33.3 | 3 | 4.48 |
| | Saline | 32 | 26.5 | 4 | 5.18 |
| Longtudinal Sulcus | EAE | 10 | 50.4 | 3 | 9.42 |
| | | 32 | 30.9 | 4 | 2.33 |
| | | 63 | 27.7 | 3 | 3.82 |
| | Saline | 32 | 16.4 | 4 | 2.42 |

EAE-experimental autoimmune encephalomyelitis; N-number animals, SEM-standard error mean; dPI-days post induction. Brain cryosections were immune-stained for Iba1 and imaged. The mean density of cells/0.1mm$^2$ was measured.

hyper-intense signal at the spine or brain surface. (Weise and Stoll, 2012; Chin et al., 2009) These uncharacterized observations were coincident with early visible biomarkers of meningeal inflammation such as TNF expression, T cell activation, etc. (Kivisakk et al., 2009; Brown and Sawchenko, 2007). In the early stages of the disease EAE-MOG brains have been shown to exhibit the presence of the active inflammatory cells at the meninges within 24 h of induction (Christy et al., 2013).

Similarly, meningeal layers of MS patients exhibit presence of germinal follicular structures acting as B cell and dendritic immune cell maturation sites (Aloisi and Pujol-Borrell, 2006; Serafini et al., 2004). These sites have been proposed to develop presence of reactive fibroblasts and collagen deposition through the process of inflammation (Zurawski et al., 2017). These germinal structures initiated by T cell activation have been found in EAE mice brain meninges as well (Magliozzi et al., 2004). It has been suggested that these sites facilitate accumulation of small amounts of gadolinium CA within the subarachnoid space (Aloisi and Pujol-Borrell, 2006; Zurawski et al., 2017). This accumulated gadolinium is reliably detected as LMCE in MS patients due to high level of CA signal sensitivity afforded by 3D-FLAIR MRI sequence (Zivadinov et al., 2018).

Therefore, we hypothesized that gadolinium-based CA will be retained in the EAE brain meninges as well, and could be imaged with ultra-high field MRI scanning. In agreement with our hypothesis, EAE-MOG animal brain meninges showed signal increase as early at 5 to 7 dPI, with peak signal 10 days before they suffered from clinical disability. This suggests that gadolinium-based CA was retained in the meninges at timepoints which coincided with the inflammatory processes requisite for generation of the disease (Brown and Sawchenko, 2007). This is in agreement with recently published 3D confocal imaging of the spinal meninges in EAE mice which showed inflammation to precede the clinical manifestation of the symptom (Shrestha et al., 2017). Decreased MRI signal in the meninges for later timepoints in

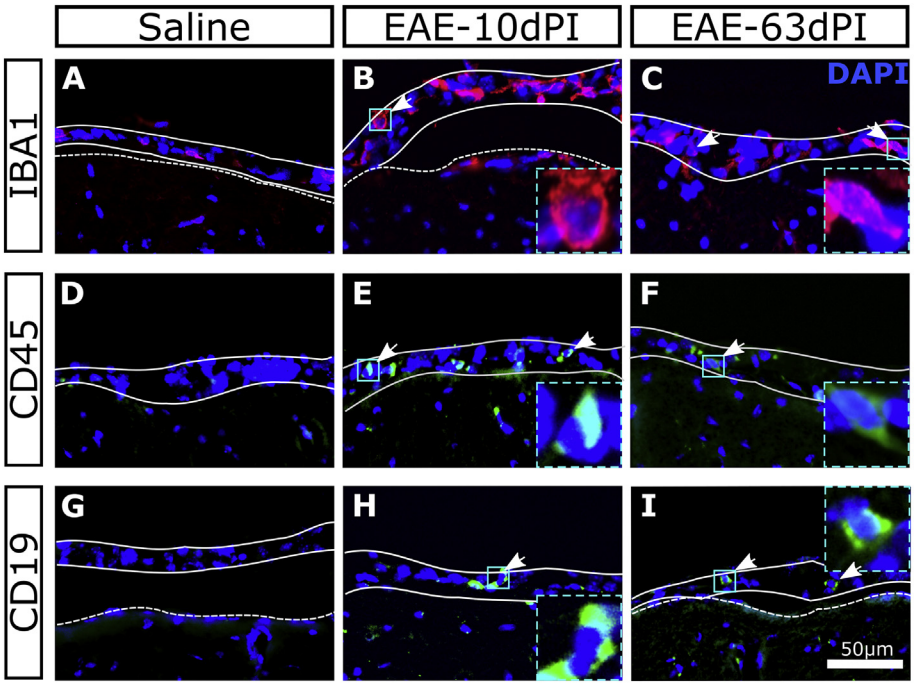


**Fig. 3.** Characterization of inflammatory cells at the meninges.
Brain sections were stained with markers of macrophage (Iba1), T (CD45) and B (CD19) cells to detect their presence in meningeal layer. (A–C) show Iba1 stained representative images from saline, 10 dPI and 63 dPI EAE brain sections respectively. (D–F) show Iba1 stained representative images from saline, 10 dPI and 63 dPI EAE brain sections respectively. (G–I) show Iba1 stained representative images from saline, 10 dPI and 63 dPI EAE brain sections respectively. White arrows point detected example cells. The cyan solid box indicates the location of the inset in the original image and dotted cyan boxes represent inset at 10× magnification. Solid white lines indicate the edges of the meningeal layer and the dotted line indicate the brain parenchyma border in images with meninges separated from brain parenchyma. *Scale is 50* μm. (For interpretation of the references to colour in this figure legend, the reader is referred to the web version of this article.)

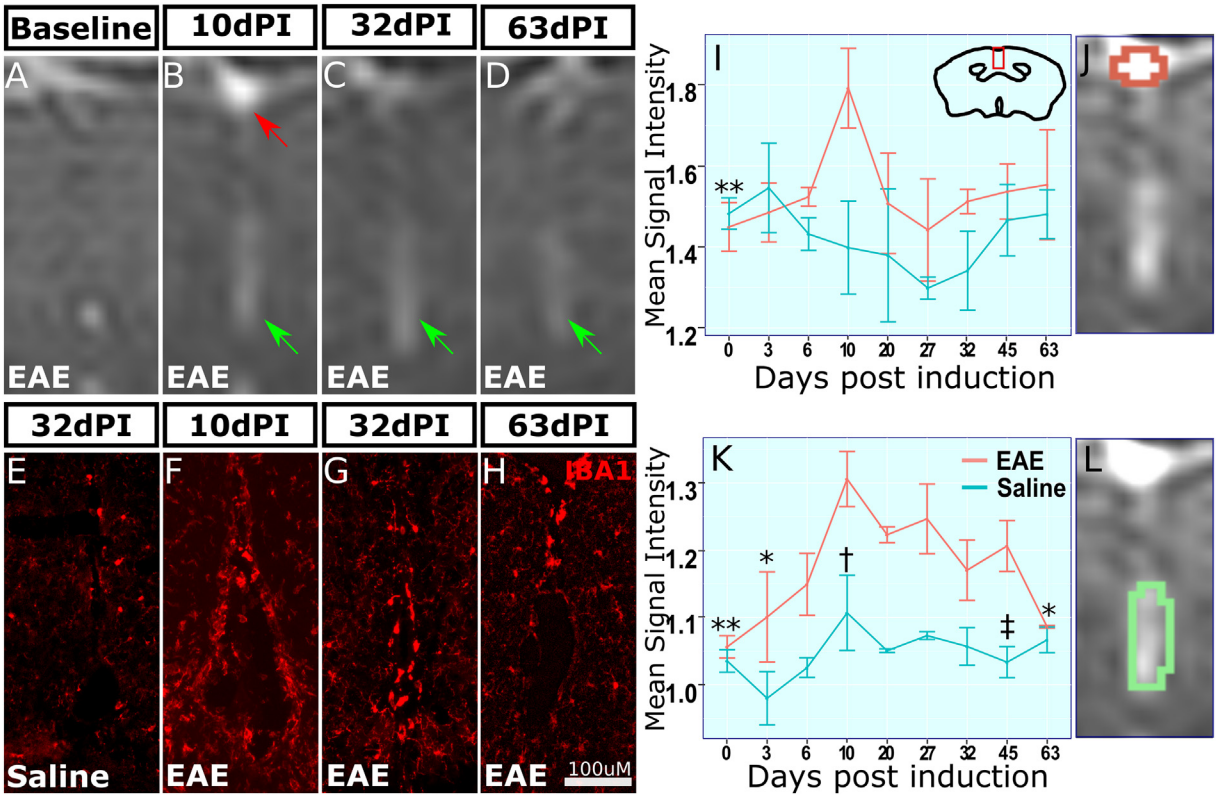


**Fig. 4.** 2D-fluid attenuated inversion recovery (FLAIR) rapid acquisition relaxation-enhanced (RARE) signal shows gadolinium-based contrast agent signal intensity retention in experimental autoimmune encephalomyelitis myelin oligodendrocyte glycoprotein (EAE-MOG) major brain veins. (A–D) show stage matched enlarged view for slices showing sagittal sinus vein in EAE brain at baseline, 10 days and 27 days timepoint (red arrow). Green is arrow pointing at the longitudinal gadolinium intensity at the longitudinal sulcus. (E–H) show representative images of brain sections at the inferior fold of the longitudinal sulcus above the corpus callosum. The sections were labeled with IBA1 to identify reactive immune and microglial cells. (I) shows the mean label intensity measured in the sagittal sinus. Inset is a black outline of a coronal brain section with red box showing where the representative images were captured. (J) shows one of the three slices with sagittal sinus label outline (orange). (K) shows mean label signal intensity at the longitudinal sulcus. (L) shows the slice with longitudinal sulcus label outline. *$p < .05$ and **$p < .01$, *'Students t-test for comparison with 10 dPI EAE signal. †$p < .05$ and, ‡$p < .01$, Students t-test for in EAE vs saline comparisons at matching timepoints. Error bars: Standard error of the mean.*
Scale is 100 μm. (For interpretation of the references to colour in this figure legend, the reader is referred to the web version of this article.)

EAE after peaking of the disease activity suggests that high MRI signal was associated only with initial inflammatory and infiltration stages of the disease. It will be interesting to characterize the MRI signal changes with time in relapsing preclinical model of EAE (McRae et al., 1992).

Histological characterization further suggests that MRI signal source is associated with initial EAE disease process within the meninges. We detected higher density of Iba1 positive microglia in the subpial brain regions. Iba1 positive cell density also mirrored the increase in the signal measures at baseline vs 10 dPI. Additionally, the EAE mouse meningeal layer sporadically presented CD45 (Greter et al., 2005) labeled T cells and CD19 (Matsushita et al., 2008) labeled B cells. Also, in agreement with published observations, the EAE mouse brain meninges presented with clusters of Iba1 positive macrophage cells (Kanazawa et al., 2002) (Ajami et al., 2011). This supports the idea that the immune cell driven changes in the meningeal layers are responsible for gadolinium accumulation and increased signal intensity (Zurawski et al., 2017).

We also found that EAE animals were exhibiting distinct signal at the major blood vessels such as sagittal sinus and Great vein of Galen. It has been suggested that T cells may enter CNS through leaky vascular-endothelial layer in EAE-MOG mice. For example, vascular endothelial integrity gene PCAM1 suppression lead to earlier EAE disease onset (Graesser et al., 2002). On similar lines, EAE mice were shown to exhibit the leaky blood vessels by day 10 dPI (Graesser et al., 2002). In agreement with these studies, our study showed that the sagittal sinus, which drains blood away from all the major blood veins in the meninges (Dorr et al., 2007), was distinctly visible at the peak inflammation phase of the disease. Therefore, increase of gadolinium-based CA signal intensity in vascular areas would suggest that in the EAE brains these blood vessels are enlarged and inflamed.

It has been shown that subpial and intra-cortical lesions in MS patients (Bo et al., 2003; Calabrese et al., 2009; Roosendaal et al., 2009), may be initiated by intrathecal immune response mediated by meningeal inflammation. (Serafini et al., 2004; Choi et al., 2012; Howell et al., 2011; Kooi et al., 2009; Magliozzi et al., 2007; Popescu and Lucchinetti, 2012; Serafini et al., 2007) Therefore, assessment of LMCE has been increasingly used as a potential marker of cortical pathology (Absinta et al., 2015; Bertolino et al., 2017; Makshakov et al., 2017). In order to better define LMCE in pre-clinical model of demyelination in-vivo, we used longitudinal MRI scanning to detect LMCE within EAE brain. We found that gadolinium-based CA signal was localized to the longitudinal sulcus of the EAE brain which anatomically resembles the human brain sulci. We noted significant gadolinium-based CA signal intensity in EAE brain longitudinal sulcus earliest, as of 3dPI, and this finding was associated with higher Iba1 stained cell density. This suggests that presence of LMCE in EAE-MOG mice, biologically resembles the follicular structures implied in LMCE images of MS patients. Histological assessment of early timepoints and determination of immune cell population at this site would further aid in confirming this hypothesis. Furthermore, it will be relevant to characterize the development of LMCE in EAE mice model with focal lesions mediated cortical demyelination in future studies. (Merkler et al., 2006)

In conclusion, we have presented a novel methodology for MRI scan based imaging of leptomeningeal inflammation in EAE-MOG brain. Our findings showed that EAE brains exhibited retention of gadolinium-based CA at early sites of inflammation, which was associated with high inflammatory cell density. Our work has implications for in-vivo serial MRI LMCE tracking of EAE disease progression in relation to different immune system modulating therapies.

## References


Abiraman, K., Pol, S.U., O'Bara, M.A., Chen, G.D., Khaku, Z.M., Wang, J., Thorn, D., Vedia, B.H., Ekwegbalu, E.C., Li, J.X., Salvi, R.J., Sim, F.J., 2015. Anti-muscarinic adjunct therapy accelerates functional human oligodendrocyte repair. J. Neurosci. 35, 3676–3688.

Absinta, M., Vuolo, L., Rao, A., Nair, G., Sati, P., Cortese, I.C., Ohayon, J., Fenton, K., Reyes-Mantilla, M.I., Maric, D., Calabresi, P.A., Butman, J.A., Pardo, C.A., Reich, D.S., 2015. Gadolinium-based MRI characterization of leptomeningeal inflammation in multiple sclerosis. Neurology 85, 18–28.

Ajami, B., Bennett, J.L., Krieger, C., McNagny, K.M., Rossi, F.M., 2011. Infiltrating monocytes trigger EAE progression, but do not contribute to the resident microglia pool. Nat. Neurosci. 14, 1142–1149.

Aloisi, F., Pujol-Borrell, R., 2006. Lymphoid neogenesis in chronic inflammatory diseases. Nat. Rev. Immunol. 6, 205–217.

Bertolino, N., Pol, S., Zivadinov, R., Babek, N., Sudyn, M., Sveinsson, M., Siebert, Danielle, Preda, Marilena, Shah, Dhaval, Schweser, F., 2017. Preclinical detection of leptomeningeal inflammation using contrast-enhanced FLAIR at 9.4T in the EAE-MOG mouse model of Multiple Sclerosis. In: Proceedings at International Society for Magnetic Resonance in Medicine, Honolulu, HI. Vol. 25. pp. 4088.

Bo, L., Vedeler, C.A., Nyland, H.I., Trapp, B.D., Mork, S.J., 2003. Subpial demyelination in the cerebral cortex of multiple sclerosis patients. J. Neuropathol. Exp. Neurol. 62, 723–732.

Brown, D.A., Sawchenko, P.E., 2007. Time course and distribution of inflammatory and neurodegenerative events suggest structural bases for the pathogenesis of experimental autoimmune encephalomyelitis. J. Comp. Neurol. 502, 236–260.

Calabrese, M., Agosta, F., Rinaldi, F., Mattisi, I., Grossi, P., Favaretto, A., Atzori, M., Bernardi, V., Barachino, L., Rinaldi, L., Perini, P., Gallo, P., Filippi, M., 2009. Cortical lesions and atrophy associated with cognitive impairment in relapsing-remitting multiple sclerosis. Arch. Neurol. 66, 1144–1150.

Chin, C.L., Pai, M., Bousquet, P.F., Schwartz, A.J., O'Connor, E.M., Nelson, C.M., Hradil, V.P., Cox, B.F., McRae, B.L., Fox, G.B., 2009. Distinct spatiotemporal pattern of CNS lesions revealed by USPIO-enhanced MRI in MOG-induced EAE rats implicates the involvement of spino-olivocerebellar pathways. J. Neuroimmunol. 211, 49–55.

Choi, S.R., Howell, O.W., Carassiti, D., Magliozzi, R., Gveric, D., Muraro, P.A., Nicholas, R., Roncaroli, F., Reynolds, R., 2012. Meningeal inflammation plays a role in the pathology of primary progressive multiple sclerosis. Brain 135, 2925–2937.

Christy, A.L., Walker, M.E., Hessner, M.J., Brown, M.A., 2013. Mast cell activation and neutrophil recruitment promotes early and robust inflammation in the meninges in EAE. J. Autoimmun. 42, 50–61.

Dietz, K.C., Polanco, J.J., Pol, S.U., Sim, F.J., 2016. Targeting human oligodendrocyte progenitors for myelin repair. Exp. Neurol. 283, 489–500.

Dorr, A., Sled, J.G., Kabani, N., 2007. Three-dimensional cerebral vasculature of the CBA mouse brain: a magnetic resonance imaging and micro computed tomography study. NeuroImage 35, 1409–1423.

Fournier, A.P., Quenault, A., Martinez de Lizarrondo, S., Gauberti, M., Defer, G., Vivien, D., Docagne, F., Macrez, R., 2017. Prediction of disease activity in models of multiple sclerosis by molecular magnetic resonance imaging of P-selectin. Proc. Natl. Acad. Sci. U. S. A. 114, 6116–6121.

Graesser, D., Solowiej, A., Bruckner, M., Osterweil, E., Juedes, A., Davis, S., Ruddle, N.H., Engelhardt, B., Madri, J.A., 2002. Altered vascular permeability and early onset of experimental autoimmune encephalomyelitis in PECAM-1-deficient mice. J. Clin. Invest. 109, 383–392.

Greter, M., Heppner, F.L., Lemos, M.P., Odermatt, B.M., Goebels, N., Laufer, T., Noelle, R.J., Becher, B., 2005. Dendritic cells permit immune invasion of the CNS in an animal model of multiple sclerosis. Nat. Med. 11, 328–334.

Harrison, D.M., Wang, K.Y., Fiol, J., Naunton, K., Royal 3rd, W., Hua, J., Izbudak, I., 2017. Leptomeningeal enhancement at 7T in multiple sclerosis: frequency, morphology, and relationship to cortical volume. J. Neuroimaging 27, 461–468.

Howell, O.W., Reeves, C.A., Nicholas, R., Carassiti, D., Radotra, B., Gentleman, S.M., Serafini, B., Aloisi, F., Roncaroli, F., Magliozzi, R., Reynolds, R., 2011. Meningeal inflammation is widespread and linked to cortical pathology in multiple sclerosis. Brain 134, 2755–2771.

Ito, D., Imai, Y., Ohsawa, K., Nakajima, K., Fukuuchi, Y., Kohsaka, S., 1998. Microglia-specific localisation of a novel calcium binding protein, Iba1. Brain Res. Mol. Brain Res. 57, 1–9.

Jones, M.V., Nguyen, T.T., Deboy, C.A., Griffin, J.W., Whartenby, K.A., Kerr, D.A., Calabresi, P.A., 2008. Behavioral and pathological outcomes in MOG 35-55 experimental autoimmune encephalomyelitis. J. Neuroimmunol. 199, 83–93.

Kanazawa, H., Ohsawa, K., Sasaki, Y., Kohsaka, S., Imai, Y., 2002. Macrophage/microglia-specific protein Iba1 enhances membrane ruffling and Rac activation via phospholipase C-gamma -dependent pathway. J. Biol. Chem. 277, 20026–20032.

Kivisakk, P., Imitola, J., Rasmussen, S., Elyaman, W., Zhu, B., Ransohoff, R.M., Khoury, S.J., 2009. Localizing central nervous system immune surveillance: meningeal antigen-presenting cells activate T cells during experimental autoimmune encephalomyelitis. Ann. Neurol. 65, 457–469.

Kooi, E.J., Geurts, J.J., van Horssen, J., Bo, L., van der Valk, P., 2009. Meningeal inflammation is not associated with cortical demyelination in chronic multiple sclerosis. J. Neuropathol. Exp. Neurol. 68, 1021–1028.

Ladewig, G., Jestaedt, L., Misselwitz, B., Solymosi, L., Toyka, K., Bendszus, M., Stoll, G., 2009. Spatial diversity of blood-brain barrier alteration and macrophage invasion in experimental autoimmune encephalomyelitis: a comparative MRI study. Exp. Neurol. 220, 207–211.

Louveau, A., Smirnov, I., Keyes, T.J., Eccles, J.D., Rouhani, S.J., Peske, J.D., Derecki, N.C., Castle, D., Mandell, J.W., Lee, K.S., Harris, T.H., Kipnis, J., 2015. Structural and functional features of central nervous system lymphatic vessels. Nature 523, 337–341.

Magliozzi, R., Columba-Cabezas, S., Serafini, B., Aloisi, F., 2004. Intracerebral expression of CXCL13 and BAFF is accompanied by formation of lymphoid follicle-like structures in the meninges of mice with relapsing experimental autoimmune encephalomyelitis. J. Neuroimmunol. 148, 11–23.

Magliozzi, R., Howell, O., Vora, A., Serafini, B., Nicholas, R., Puopolo, M., Reynolds, R.,

Aloisi, F., 2007. Meningeal B-cell follicles in secondary progressive multiple sclerosis associate with early onset of disease and severe cortical pathology. Brain 130, 1089–1104.
Makshakov, G., Magonov, E., Totolyan, N., Nazarov, V., Lapin, S., Mazing, A., Verbitskaya, E., Trofimova, T., Krasnov, V., Shumilina, M., Skoromets, A., Evdoshenko, E., 2017. Leptomeningeal contrast enhancement is associated with disability progression and grey matter atrophy in multiple sclerosis. Neurol. Res. Int. 2017, 8652463.
Mardiguian, S., Serres, S., Ladds, E., Campbell, S.J., Wilainam, P., McFadyen, C., McAteer, M., Choudhury, R.P., Smith, P., Saunders, F., Watt, G., Sibson, N.R., Anthony, D.C., 2013. Anti-IL-17A treatment reduces clinical score and VCAM-1 expression detected by in vivo magnetic resonance imaging in chronic relapsing EAE ABH mice. Am. J. Pathol. 182, 2071–2081.
Matsushita, T., Yanaba, K., Bouaziz, J.D., Fujimoto, M., Tedder, T.F., 2008. Regulatory B cells inhibit EAE initiation in mice while other B cells promote disease progression. J. Clin. Invest. 118, 3420–3430.
McFarland, H.F., Martin, R., 2007. Multiple sclerosis: a complicated picture of autoimmunity. Nat. Immunol. 8, 913–919.
McRae, B.L., Kennedy, M.K., Tan, L.J., Dal Canto, M.C., Picha, K.S., Miller, S.D., 1992. Induction of active and adoptive relapsing experimental autoimmune encephalomyelitis (EAE) using an encephalitogenic epitope of proteolipid protein. J. Neuroimmunol. 38, 229–240.
Merkler, D., Ernsting, T., Kerschensteiner, M., Bruck, W., Stadelmann, C., 2006. A new focal EAE model of cortical demyelination: multiple sclerosis-like lesions with rapid resolution of inflammation and extensive remyelination. Brain 129, 1972–1983.
Petry, K.G., Brochet, B., Dousset, V., Vignes, J.R., Boiziau, C., 2010. Inflammation induced neurological handicap processes in multiple sclerosis: new insights from preclinical studies. J. Neural Transm. (Vienna) 117, 907–917.
Popescu, B.F., Lucchinetti, C.F., 2012. Meningeal and cortical grey matter pathology in multiple sclerosis. BMC Neurol. 12, 11.
Ransohoff, R.M., Kivisakk, P., Kidd, G., 2003. Three or more routes for leukocyte migration into the central nervous system. Nat. Rev. Immunol. 3, 569–581.
Roosendaal, S.D., Moraal, B., Pouwels, P.J., Vrenken, H., Castelijns, J.A., Barkhof, F., Geurts, J.J., 2009. Accumulation of cortical lesions in MS: relation with cognitive impairment. Mult. Scler. 15, 708–714.
Serafini, B., Rosicarelli, B., Magliozzi, R., Stigliano, E., Aloisi, F., 2004. Detection of ectopic B-cell follicles with germinal centers in the meninges of patients with secondary progressive multiple sclerosis. Brain Pathol. 14, 164–174.
Serafini, B., Rosicarelli, B., Franciotta, D., Magliozzi, R., Reynolds, R., Cinque, P., Andreoni, L., Trivedi, P., Salvetti, M., Faggioni, A., Aloisi, F., 2007. Dysregulated Epstein-Barr virus infection in the multiple sclerosis brain. J. Exp. Med. 204, 2899–2912.
Shrestha, B., Jiang, X., Ge, S., Paul, D., Chianchiano, P., Pachter, J.S., 2017. Spatiotemporal resolution of spinal meningeal and parenchymal inflammation during experimental autoimmune encephalomyelitis. Neurobiol. Dis. 108, 159–172.
Stoll, G., Bendszus, M., 2009. Imaging of inflammation in the peripheral and central nervous system by magnetic resonance imaging. Neuroscience 158, 1151–1160.
Weise, G., Stoll, G., 2012. Magnetic resonance imaging of blood brain/nerve barrier dysfunction and leukocyte infiltration: closely related or discordant? Front. Neurol. 3, 178.
Zivadinov, R., Ramasamy, D.P., Hagemeier, J., Kolb, C., Bergsland, N., Schweser, F., Dwyer, M.G., Weinstock-Guttman, B., Hojnacki, D., 2018. Evaluation of leptomeningeal contrast enhancement using pre-and postcontrast subtraction 3D-FLAIR imaging in multiple sclerosis. AJNR Am. J. Neuroradiol. 39 (4), 642–647.
Zurawski, J., Lassmann, H., Bakshi, R., 2017. Use of magnetic resonance imaging to visualize leptomeningeal inflammation in patients with multiple sclerosis: a review. JAMA Neurol. 74, 100–109.